ROMANIAN JOURNAL OF INFORMATION SCIENCE AND TECHNOLOGY
Volume 19, Number 3, 2016, 295–308

High Accuracy Amperometric Sense and Control Circuit for Three-electrode Biosensors

Andrei ENACHE[1], Ion RUSU[1], Florin DRĂGHICI[1], Gheorghe PRISTAVU[1], Gheorghe BREZEANU[1], and Florin ENACHE[2]

[1]University Politehnica of Bucharest, Romania
Email: andrei_e93@yahoo.com, romcarfem@yahoo.com, f_draghici@yahoo.com, gheorghe_pristavu@yahoo.com, gheorghe.brezeanu@dce.pub.ro
[2]Military Technical Academy, Bucharest, Romania
Email: florinre@yahoo.com

Abstract. A system used for measuring the concentration of chemical compounds in fluids/solutions is designed, implemented and tested. The system comprises a Sense and Control Circuit formed with a potentiostat for three-electrode electrochemical cell (biosensor) biasing and a transimpedance amplifier for cell current processing. The stability of the potentiostat and the linearity of the transimpedance amplifier are theoretically and experimentally investigated. The high accuracy of the system is demonstrated by simulations and measurements. A comparison with a commercially available system is carried out.

Keywords: biosensor, potentiostat, amperometry, stability, frequency compensation.

1 Introduction

Determining the concentration of chemical compounds is required in several applications, such as the evaluation of glucose and alcohol concentrations in beverages, glucose and lactate in blood [1], [2], gas concentration [3] etc.

Electrochemical sensing can be used for such measurements, in either of its three forms [4]: conductometric (also known as Electrochemical Impedance Spectroscopy [5]), amperometric and potentiometric (voltammetry [6]).

In this paper, a concentration measurement system based on amperometric electrochemical sensing using a three-electrode electrochemical cell [7] is presented. In this case, a constant voltage is applied between two of the cell electrodes and the resulting faradaic current, proportional to the concentration of a chemical compound, is read out from the third electrode [4] [8] [9].

The proposed system is composed of analog and digital blocks [10]. The analog part (Sense and Control Circuit SCC) is conceived for high linearity over a wide range

of input signals, which allows it to be used with a large array of sensing elements (biosensors). Furthermore, it is designed for high accuracy, with special regard to noise immunity and stability. The digital block is introduced in order to allow convenient control of the system. The SCC performances are proven by analytical and numerical determinations, as well as through experimental investigations.

A more detailed exposition of the concentration measurement system is given, pertaining in particular to the power supply and its design based on noise considerations, in comparison with our previous paper [10]. An in-depth presentation of the analog block is given, especially regarding design considerations. The stability study [10] is expanded upon with the inclusion of an analytical model, allowing a more thorough analysis of the analog block's frequency behavior.

Comparative measurements with a portable system (PG580) are presented, validating the proposed circuits performances. A very good agreement between the output characteristics of the compared solutions is evinced.

2 System Description

The block diagram of the proposed amperometric concentration measurement system is shown in **Fig. 1.**

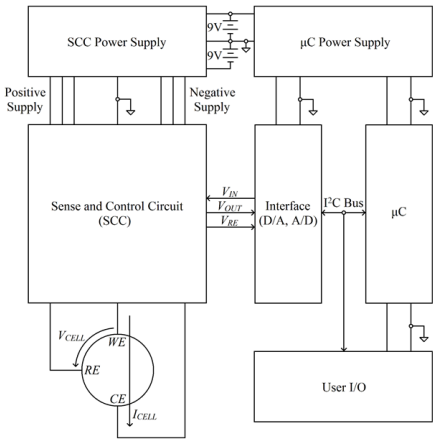

Fig. 1: Block diagram of the concentration measurement system.

The sensing element of the system is a three-electrode electrochemical cell [2], [11], whose operation is based on redox reactions [12]. The cell's electrodes are [11]: Working Electrode (*WE* – on which an enzyme is deposed and where the reaction takes place), Reference Electrode (*RE* – for reaction control), Counter Electrode (*CE* – which provides the current for the reaction).

The analog core of the system, the sense and control circuit (SCC), is responsible for providing the cell with the constant voltage required for amperometric measurement (accomplished by a potentiostat circuit) and for processing the output current of the sensor (using a transimpedance amplifier) [11].

The SCC has a power supply separate from the supply of the digital part of the system, due to noise considerations. The implementation of the power supply using batteries increases noise robustness and stability [11].

The digital block is based on a microcontroller (μC), which is accompanied by D/A and A/D converters, used for interfacing with the SCC, and I/O peripherals for accepting user commands and displaying measurement results.

For measuring the concentration of a compound, the enzyme is deposited on *WE*, a constant voltage $V_{CELL} = V_{WE} - V_{RE}$ is applied on the cell by the potentiostat and the cell is dipped in the solution of interest. The polarity of V_{CELL} determines the type of electrochemical reaction that takes place (oxidation, if $V_{CELL} > 0$, reduction, if $V_{CELL} < 0$ [11]). The solution is agitated in order to maintain homogeneity while the reaction occurs, which leads to the generation of low-frequency noise in the cell.

The user is allowed to set the value of the desired V_{CELL} voltage (corresponding to a certain compound), which the μC system provides to the biosensor via the SCC block. As a result of the electrochemical reaction which takes place on the *WE* electrode, a low-value current I_{CELL} is generated between *WE* and *CE* (if oxidation occurs *CE* sources I_{CELL}, whilst in the case of reduction *CE* sinks I_{CELL} [11]). The SCC's transimpedance amplifier converts this small current into a voltage (V_{OUT}). This output voltage increases with the compound concentration. The μC acquires this voltage via an A/D converter and based on its value calculates and displays the cell current.

3 Sense and Control Circuit (SCC)

3.1 Circuit overview

The proposed SCC circuit, shown in **Fig. 2.**, is based on a standard two-blocks schematic [12]. The potentiostat block ensures a constant V_{CELL} voltage between *WE* and *RE*. The resulting biosensor current, I_{CELL}, is amplified by the second block, a simple transimpedance amplifier.

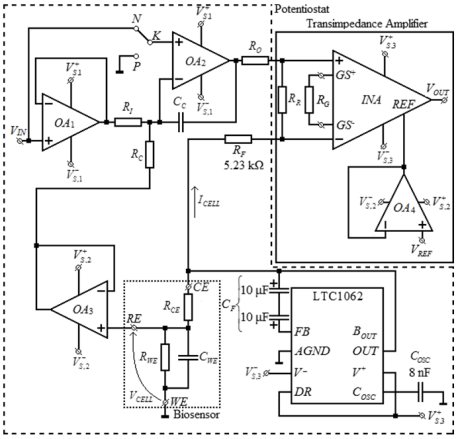

Fig. 2: Sense and control circuit topology.

The three-electrode electrochemical cell (biosensor – **Fig. 2**) was substituted by its equivalent Randles schematic [2], [11]. The most significant part of this equivalent circuit is represented by $R_{WE} - C_{WE}$ impedance, which models the electrochemical reaction (reduction or oxidation). R_{CE} is the solution resistance seen between the reference electrode (*RE*) and the counter electrode (*CE*).

In the circuit shown in **Fig. 2**, the potentiostat comprises three operational amplifiers ($OA_1 - OA_3$) and a 5^{th} order low-pass filter, with a cutoff frequency of 5 Hz (R_F, C_F, C_{OSC}, LTC1062) [13]. The inclusion of this filter is crucial, because it practically eliminates high-frequency and agitator noise from the feedback loop, while not affecting the value of I_{CELL}.

The essential operational amplifier in the potentiostat is OA_2, which ensures the constant and stable value of the cell voltage, determining the generation of I_{CELL}. Because OA_2's feedback loop contains a highly capacitive sensor as well as the 5^{th} order low-pass filter (which causes large negative phase shifts), a compensation circuit (formed with C_C, R_I and R_C) was included. This negative feedback loop ensures the same potentials at OA_2's inputs.

Because I_{CELL} is read out from the *CE* electrode, no current should be contributed by *RE*. As such, the introduction of R_I and R_C into the circuit determines the necessity of using a voltage buffer, OA_3, to separate the *RE* electrode of the cell from the resistances.

OA_1 was added in order to increase the potentiostat's input resistance. The input voltage of the SCC (V_{IN}) is obtained using a single-supply D/A converter (which provides only positive voltages). Since *WE* is connected to ground (requiring a negative RE voltage in order to obtain $V_{CELL} > 0$) the *K* switch was included.

When *K* is on the *N* position, the potentiostat copies V_{IN} at both R_I terminals. There is no current flow through R_I and R_C and the input voltage is repeated on the *RE* electrode, resulting in $V_{CELL} = -V_{IN} < 0$.

When *K* is on the *P* position, the potentiostat behaves similarly to an inverting operational amplifier configuration whose output is at *RE*. R_I and R_C are chosen to be equal, resulting in a gain (V_{RE}/V_{IN}) of -1. As such, the input voltage is copied at the *RE* electrode, but with inverted polarity, meaning $V_{CELL} = V_{IN} > 0$.

The transimpedance amplifier is required to convert and increase the typically very low values of I_{CELL} to processable levels. The voltage resulting from the cell current passing through R_R is amplified by the instrumentation amplifier *(INA)*:

$$V_{OUT} = -G \cdot R_R \cdot I_{CELL} + V_{REF} \tag{1}$$

where *G* is the gain of the instrumentation amplifier (set by R_G) and V_{REF} is the reference voltage for the output of the amplifier.

3.2 SCC Power Supply Circuit

The circuit used for supplying power to the SCC is shown in **Fig. 3**.

As seen in **Fig. 3**, all the integrated circuits in the SCC are powered from a differential supply, with the two voltages being obtained from the 9V batteries using fixed +5V and -5V regulators.

Filtering the power supply voltages using RC low-pass filters with low cut-off frequencies (several Hz) is done to reduce noise - either produced by the regulators or by electromagnetic fields in the surrounding environment. The ladder structure of the filters, with only two circuits powered at each stage, was chosen in order to ensure that noise isn't transferred between circuits through the power supply lines.

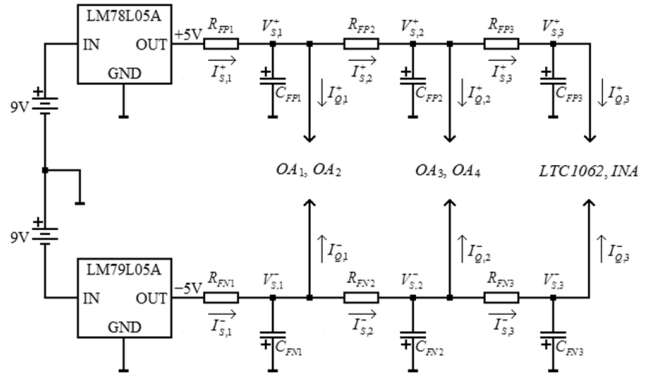

Fig. 3: SCC power supply circuit.

3.3 Potentiostat stability

The stability of the circuit is conditioned by OA_2 and its complex negative feedback loop. In order to evaluate stability, the loop transmission was considered, given by [14]:

$$T(\omega) = A_d(\omega) \cdot \beta(\omega) \tag{2}$$

where $A_d(\omega)$ represents the differential mode small signal gain of OA_2 and $\beta(\omega)$ represents the feedback loop transfer function (from the output of OA_2 to its inverting input). This loop includes the LTC1062 circuit (**Fig. 2**), for which a numerical model does not exist. Thus, only an analytical method can be utilized to determine transmission.

For this approach, the filter configuration in **Fig. 4** is considered, representing a 5^{th} order low-pass filter with a cutoff frequency of 5 Hz and a maximally flat passband response [13]. The transfer function of this filter, denoted herein by H(ω), was considered to have a simple form, given by:

$$H(\omega) = \frac{V_{OUT,F}(\omega)}{V_{IN,F}(\omega)} = \frac{1}{\left(1 + j\frac{\omega}{\omega_f}\right)^5}, \omega_f = 2\pi \cdot 5Hz \tag{3}$$

The expression corresponds to the particular situation in which the filter's input ($v_{IN,F}$) is driven by an ideal voltage source and its output ($v_{OUT,F}$) is open. The proposed SCC circuit (**Fig. 2**) includes a load for this filter, represented by the biosensor, while at the input there are two resistances (R_O, R_R) in series with R_F towards a voltage source (OA_2). Therefore, in order to obtain accurate expressions for $\beta(\omega)$ and T(ω), the transfer function of LTC1062 from OUT to FB (denoted by G(ω)) is used instead:

$$G(\omega) = \frac{V_{FB}(\omega)}{V_{OUT,F}(\omega)} = \frac{H(\omega) \cdot (1 + j\omega R_F C_F) - 1}{H(\omega) \cdot j\omega R_F C_F} - 1 \tag{4}$$

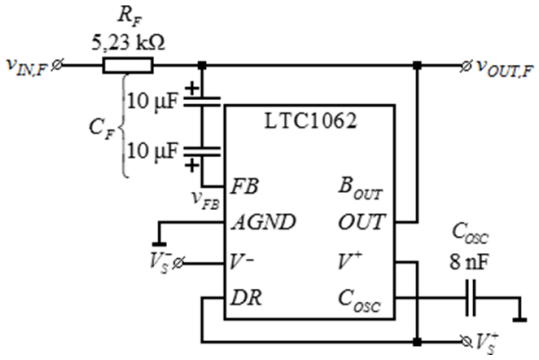

Fig. 4: 5^{th} order 5 Hz low-pass filter formed with LTC1062.

Under these approximations, the following expression is obtained for the loop transfer function:

$$\beta(\omega) = \frac{j\omega\frac{R_C C_C}{2}}{1+j\omega\frac{R_C C_C}{2}} + \frac{1}{2}\cdot\frac{1}{1+\frac{j\omega}{2\pi\cdot GBW_3}}\cdot\frac{R_{WE}}{R_{WE}+R_{CE}+j\omega R_{WE}R_{CE}C_{WE}}\cdot$$
$$\frac{1}{1+j\omega\frac{R_C C_C}{2}}\cdot\frac{1}{\frac{R_O+R_R+R_F}{R_{CE}+\frac{R_{WE}}{1+j\omega R_{WE}C_{WE}}}+1-j\omega C_F\cdot(R_O+R_R+R_F)\cdot[G(\omega)-1]}, \tag{5}$$

where GBW_3 is the gain-bandwidth product of OA_3.

Eq. (5) evinces two phase-loop contributors: the compensation circuit (R_I, R_C, C_C) (first term in (5)) and the branch which includes the sensor (second term). The presence of LTC1062's transfer function (G(ω)) in (5) causes phase to drop rapidly at low frequencies. Hence, to ensure stability, the compensation capacitor's contribution should be dominant in determining $\beta(\omega)$ phase at higher frequencies (where the filter's phase shift is significant).

Considering cell equivalent element values: $R_{WE} = 1\ M\Omega$, $C_{WE} = 1\ \mu F$ and $R_{CE} = 100\ \Omega$, the plots in **Fig. 5** (magnitude) and **Fig. 6** (phase) were obtained.

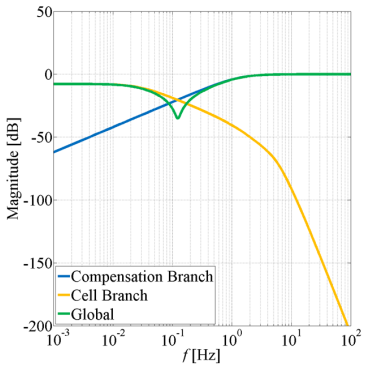

Fig. 5: Feedback loop transfer function magnitude plot.

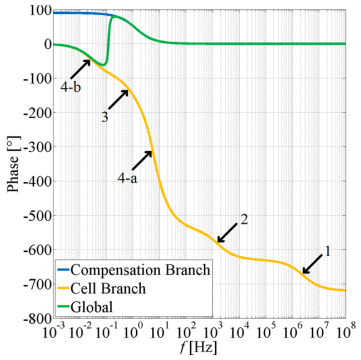

Fig. 6: Feedback loop transfer function phase plot.

In **Fig. 6**, it can be seen that the second term from eq. (5) (corresponding to the cell branch, represented by the yellow line in **Fig. 6**) has a phase of $-720°$ at 100 MHz. This result corresponds to the presence of 8 poles up to this frequency, due to:

1. first factor – a simple pole determined by the OA_3 buffer;
2. second factor – a 1^{st} order pole caused by the electrochemical cell;
3. third factor – a simple pole introduced by the compensation circuit;
4. fourth factor – a 4^{th} order pole at 5 Hz (a) and another pole at lower frequencies (b) – tens of mHz.

Regarding the fourth factor, the lowest frequency pole (4-b – **Fig. 6**) appears due to the non-ideal filter operation (regarding drive voltage and load). This effect was identified by substituting G(ω), given by (4), into (5):

$$\beta(\omega) = \frac{j\omega\frac{R_C C_C}{2}}{1+j\omega\frac{R_C C_C}{2}} + \frac{1}{2}\cdot\frac{1}{1+j\omega\frac{R_C C_C}{2}}\cdot\frac{R_{WE}}{R_{WE}+R_{CE}+j\omega R_{WE}R_{CE}C_{WE}}\cdot \frac{1}{\frac{R_O+R_R+R_F}{R_{CE}+\frac{R_{WE}}{1+j\omega R_{WE}C_{WE}}} - \frac{R_O+R_R}{R_F} + \frac{R_O+R_R+R_F}{R_F}\cdot\frac{1}{H(\omega)}}\cdot\frac{1}{1+\frac{j\omega}{2\pi\cdot GBW_3}} \tag{6}$$

The transfer function of the circuit from OA_2 output to OA_3 input, which is included in the second term of relation (6) is given by:

$$F(\omega) = \frac{V_{RE}(\omega)}{V_{OA_2}(\omega)} = \frac{R_{WE}}{R_{WE}+R_{CE}+j\omega R_{WE}R_{CE}C_{WE}}\cdot \frac{1}{\frac{R_O+R_R+R_F}{R_{CE}+\frac{R_{WE}}{1+j\omega R_{WE}C_{WE}}} - \frac{R_O+R_R}{R_F} + \frac{R_O+R_R+R_F}{R_F}\cdot\frac{1}{H(\omega)}} \tag{7}$$

If only the filter (**Fig. 4**) were connected between OA_2 and OA_3 in **Fig. 2**, meaning $R_O = R_R = R_{CE} = 0$, $R_{WE} = \infty$ and $C_{WE} = 0$, it would operate under datasheet conditions [13]. Replacing these values in eq. (7) yields:

$$F(\omega) = H(\omega) \tag{8}$$

which is the expected result. Thus, the validity of the stability analysis is demonstrated. Furthermore, it can be seen in relation (7) that $H(\omega)$ (filter transfer function in the ideal case) appears in a more complex expression, which includes all the circuit elements that make LTC1062 operate differently from the case shown in **Fig. 4**. This explains the degeneration of the 5^{th} order 5 Hz filter pole into two poles.

The presence of the low frequency pole (4-b – **Fig. 6**) justifies the inclusion of C_C, R_I and R_C elements in the potentiostat loop. Thus, the resulting high-pass filter with low cut-off frequency short-circuits the cell branch when its phase shift drops, preventing instability (Global phase plot – **Fig. 6**).

C_C, R_I and R_C values are determined based on loop transmission phase variation, which also includes the effect of the dominant pole of OA_2 (itself determining a phase decrease at low frequencies). Considering OA_2 to be an LTC1051 operational amplifier (high DC precision amplifier) and for the same cell element values as before, the $T(\omega)$ plots in **Fig. 7** (magnitude) and **Fig. 8** (phase) are obtained. Circuit stability was achieved for $C_C = 5$ μF (two back-to-back 10 μF electrolytic capacitors) and $R_C = 50$ $k\Omega$.

In **Fig. 8**, as frequency increases, phase starts dropping because of the dominant pole of OA_2 and the low frequency pole determined by low-pass filter block formed with LTC1062. At higher frequencies, the compensation branch determines the expected phase increase. Considering that the obtained $T(\omega)$ magnitude (**Fig. 7**) is over 0 dB at working frequencies (under 5 Hz), it is essential that phase never reach $-180°$. Indeed, it can be seen that phase remains over $-135°$ (**Fig. 8**), ensuring potentiostat stability.

The previous stability analysis was reiterated for a wide domain of biosensor impedance element values (R_{WE}=0.1... 10MΩ when C_{WE}=1μF and C_{WE}=0.1...10μF when R_{WE}=1MΩ), resulting in the plots shown in **Fig. 9**. In all cases, the frequency behaviour was similar to **Fig. 7** and **Fig. 8**, with phase never dropping below $-140°$.

In **Fig. 9. a,b** it can be seen that, while the variation of R_{WE} has a significant effect on $T(\omega)$, it does not lead to instability for any of the investigated cases. Furthermore, **Fig. 9.b** shows that, as R_{WE} increases, the phase minimum asymptotically reaches a limit value. Thus, a further increase in resistance would still result in a stable circuit.

Fig. 9. c,d show that C_{WE} has a practically negligible effect on loop transmission. This illustrates another benefit of using the LTC1062 filter circuit: the dependence of loop transmission on cell impedance (particularly on C_{WE}) is significantly reduced. This is also supported by the fact that the pole determined by the electrochemical cell in the expressions of $\beta(\omega)$ and $T(\omega)$ is outside working frequencies.

In the simple case with no filter (and associated compensation circuit), analysed in [15], the loop transfer function,

$$\beta(\omega) = \frac{R_{WE}}{R_{WE} + R_{CE} + R_L} \cdot \frac{1}{1 + j\omega \cdot \frac{R_{WE}(R_{CE}+R_L)}{R_{WE}+R_{CE}+R_L} \cdot C_{WE}} \tag{9}$$

evinces a strong influence of C_{WE} on stability (the frequency of the only pole in expression (9) is determined by C_{WE}.

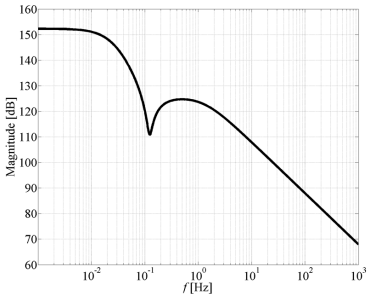

Fig. 7: Loop transmission magnitude.

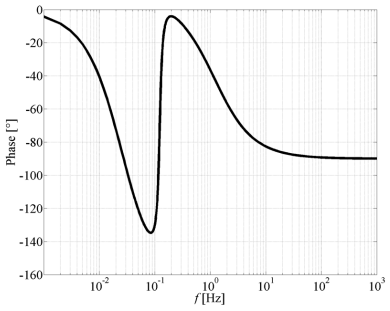

Fig. 8: Loop transmission phase.

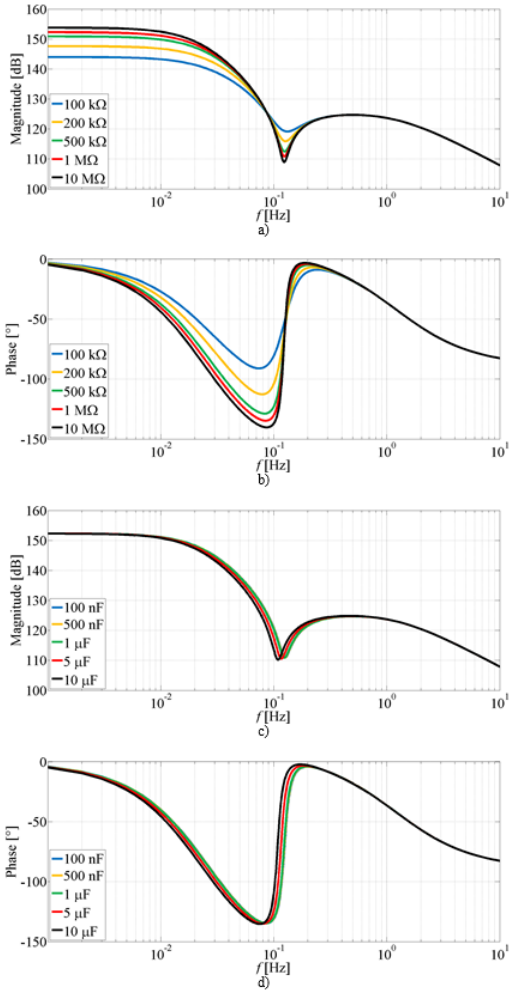

Fig. 9: Loop transmission magnitude and phase for different values of a), b) R_{WE} and c), d) C_{WE}

4 Simulation and Experimental Results

The proposed concentration measurement system (**Fig. 1**) was characterized using a PCB implementation for the analog block presented in Section 3. Measurements regarding potentiostat performance, transimpedance amplifier transfer characteristics and start-up were carried out. All investigations were performed using the equivalent Randles model for the biosensor, included in **Fig. 2**.

Fig. 10 shows the simulated variation of the cell voltage with the input voltage for multiple values of the R_{WE} resistance in the case of K switched to $N(V_{RE} > 0, V_{CELL} < 0)$.

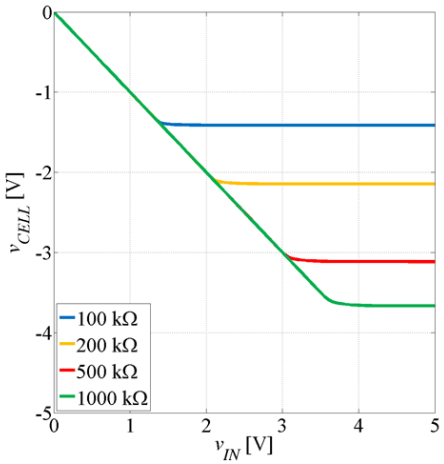

Fig. 10: Cell voltage versus input voltage for multiple values of R_{WE}.

Fig. 11 shows the simulated variation of the cell voltage with R_{WE} for V_{IN}=204.2 mV. R_{WE} variations are equivalent with different compound concentrations which need to be evaluated by the concentration measurement system.

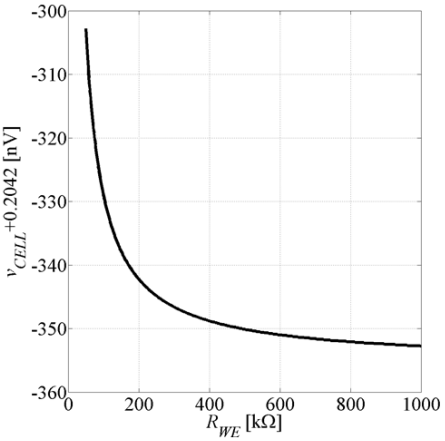

Fig. 11: Cell voltage versus cell resistance R_{WE}.

A practically constant cell voltage is demonstrated, representative of a potentiostat.

Furthermore, the DC offset error ($V_{IN} - V_{RE} = V_{IN} + V_{CELL}$) observed in the simulation in **Fig. 11** is extremely low (around -300 nV).

Fig. 12 shows the variations of the cell and output voltages at start-up (the input voltage was switched from 0 to V_{IN} = 204.2 mV at $t = 0$). This response emphasizes an initial oscillation tendency, which is dampened and eliminated by the high-pass filter. Thus, the introduction of the compensation branch is justified and validated.

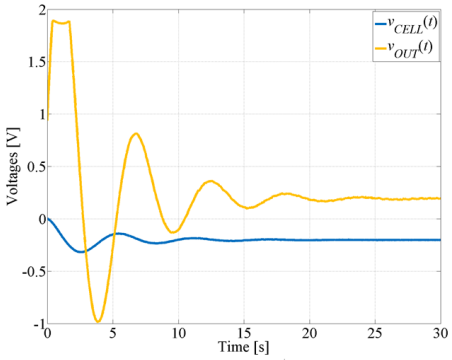

Fig. 12: Cell voltage versus cell resistance R_{WE}.

In **Fig. 13**, both simulated and measured transfer characteristics $v_{OUT} = f(i_{CELL})$ of the Sense and Control Circuit are given for two values of the input voltage (V_{IN}) in the case of *K* switched to *N* ($V_{CELL} < 0$), respectively.

The transimpedance amplifier in the SCC was designed for a gain of 1 MΩ. The output voltage decreases linearly with cell current. A very good agreement between measurement and simulation results was achieved. The excellent linearity of the analog block considerably simplifies the μC signal processing algorithms. Experimentally, no cell voltage variations were observed as the value R_{WE} was modified, because of measurement device sensitivity (simulated variations were in the order of tens of nV – **Fig. 11**).

The I_{CELL} range for which a high linearity was experimentally demonstrated is roughly 50 nA. . . 2 μA (**Fig. 13**). This current interval corresponds, for example, to an ethanol biosensor's output signal, measuring a molar concentration between 0.05 and 10.5 mM [16].

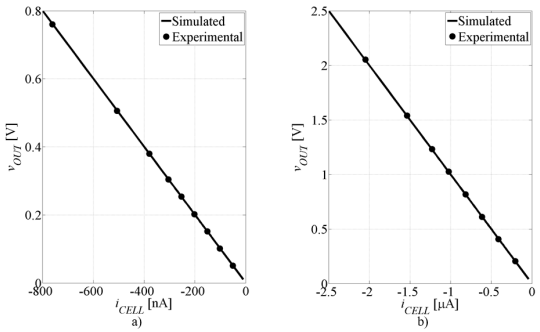

Fig. 13: Output voltage versus cell current for input voltage: a) 50.5 mV b) 204.2 mV (*K* switched to *N*, negative cell voltages).

5 SCC Performance versus a Commercial Potentiostat

The SCC operation is compared with a three-electrode cell measurement potentiostat, PG580. Measurements of I_{CELL} vs. R_{WE} were performed on the same resistor network using the two devices, in order to compare their accuracy. The group of resistors used is shown in **Fig. 14**. C_{WE} was not considered because, as previously proven (Section 3), it has a negligible effect on the SCC's operation.

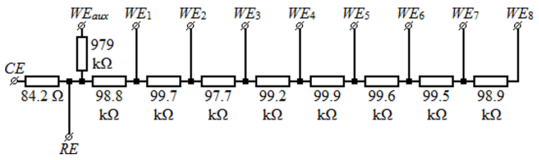

Fig. 14: Resistor network used for comparative measurements.

Fig. 15 shows the two $I_{CELL} = f(R_{WE})$ characteristics measured using our Sense and Control Circuit and PG580, respectively. The plotted cell current values were acquired differently for each measurement apparatus.

In the case of the measurements on our proposed system, a calibration is necessary. For this purpose, a linear regression was carried out on a set of measurement points (I_{CELL}, V_{OUT}). I_{CELL} was determined by dividing V_{CELL} by R_{WE}. The fitting yielded a slope, A_Z = 1.0062 MΩ, and an intercept, corresponding to the amplifier offset voltage, V_{OS} = 0.513 mV. Following the calibration process, the plotted I_{CELL} was determined based on the measured V_{OUT} voltage using the relation

$$I_{CELL} = \frac{V_{OUT} - V_{OS}}{A_Z} \tag{10}$$

The current measured with PG580 was corrected, considering the mismatch between V_{CELL} values:

$$I_{CELL,C} = I_{CELL} \cdot \frac{(V_{CELL})_{Our\ circuit}}{V_{(CELL)PG580}} \tag{11}$$

This is permissible since the difference between the two V_{CELL} values is so low that the assumption of small-signal conditions holds true.

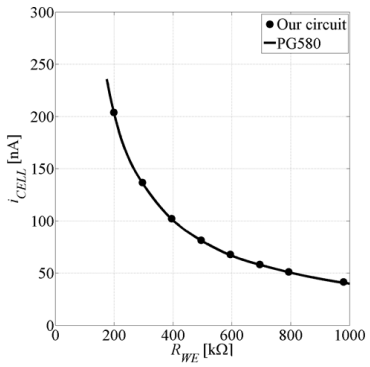

Fig. 15: Measured cell current I_{CELL} versus cell resistance R_{WE}

In **Fig. 15**, a good agreement is demonstrated between the I_{CELL} values measured with the presented concentration measurement system and the values $I_{CELL,C}$obtained using the portable device PG580.

6 Conclusions

A chemical compounds concentration measurement system was designed and implemented. The system is based on amperometric electrochemical sensing using a three-electrode cell and comprises a potentiostat for sensor bias (V_{CELL}), a transimpedance amplifier for output signal amplification (I_{CELL}) and a microcontroller module for interfacing with the user, with separate power supplies for the analog and digital blocks (due to noise considerations).

The designed Sense and Control Circuit has very good noise performance, owing to the 5^{th} order low-pass filter implemented using the LTC1062 circuit. Using this filter, however, led to concerns regarding stability, which was analytically investigated. This allowed the adequate design of the compensation circuit. The good stability was experimentally verified for multiple values of cell impedance. Note that the circuit showed an initial oscillation tendency, which was dampened and eliminated due to the proper implementation of the compensation filter. Furthermore, the potentiostat performances were confirmed by simulation and experiments. Practically constant cell voltages at values of 50.5 mV and 204.2 mV were measured.

Simulations and measurements on the transimpedance amplifier, introduced to raise output signal level, demonstrated very good linearity for a high gain (1 MΩ). This linear variation was observed for 50 nA. . . 2 μA range of cell currents.

The SCC was compared with a commercial potentiostat (PG580) with very good results. An excellent agreement of output characteristics was obtained between the two systems.

Acknowledgements. The research presented in this paper was funded by research project PNCDI II 146/2014.

References

[1]] De VENUTO D., TORRE M. D., BOERO C., CARRARA S., De MICHELI G., *A Novel Multi-Working Electrode Potentiostat for Electrochemical Detection of Metabolites*, in: Proceedings of the IEEE Sensors Conference, Waikoloa, USA, 1-4 Nov. 2010, pp. 15721577.

[2] GHOREISHIZADEH S. S., TAURINO I., CARRARA S., De MICHELI G., *A Current-Mode Potentiostat for Multi-Target Detection Tested with Different Lactate Biosensors, in: Proceedings of the IEEE Biomedical Circuits and Systems Conference*, Hsinchu, Taiwan, 28-30 Nov. 2012, pp. 128131.

[3] KUBERSKY P., KROUPA M., HAMACEK A., STULIK J., ZWIEFELHOFER V., *Potentiostat solution for electrochemical amperometric gas sensor, in: Proceedings of the 35th International Spring Seminar on Electronics Technology*, Bad Aussee, Austria, 9-13 May 2012, pp. 388393.

[4] MOHANTY S. P., KOUGIANOS E., *Biosensors: A tutorial review, in: IEEE Potentials Magazine*, Volume 25, Issue 2, March-April 2006, pp. 3540.

[5] ORAZEM M. E., TRIBOLLET B., *Electrochemical Impedance Spectroscopy, in: The Electrochemical Society Series*, John Wiley & Sons, Inc., Hoboken, New Jersey, 2008.

[6] NICHOLSON R. S., *Theory and Application of Cyclic Voltammetry for Measurement of Reaction Electrode Kinetics*, in: *Analytical Chemistry* 37, No. 11, October 1965, pp. 13511355.

[7] GRIMES C. A.,. DICKEY E. C,. PISHKO M. V., *Encyclopedia of Sensors*, American Scientific Publishers, 2006.

[8] ZIUO L., ISLAM S. K., MAHBUB I., QUAIYUM F., *A Low-Power 1-V Potentiostat for Glucose Sensors*, in: *IEEE Transactions on Circuits and Systems II: Express Briefs*, Volume 62, Issue 2, February 2015, pp. 204208.

[9] GHANABRI S., HABIBI M., *Low power potentiostat using switching technique for three electrode amperometric sensors, in: Proceedings of the 23rd Iranian Conference on Electrical Engineering*, Tehran, Iran, 10-14 May 2015, pp. 11541158.

[10] ENACHE A., RUSU I., DRĂGHICI F., BREZEANU Gh., PRISTAVU Gh., ENACHE F., *Smart sensor for chemical compounds concentrations, in: Proceedings of the International Semiconductor Conference (CAS)*, Sinaia, Romania, 10-12 Oct. 2016, pp. 201-204.

[11] AHMADI M. M., GRAHAM A. J., *Current-Mirror Based Potentiostats for Three-Electrode Amperometric Electrochemical Sensors*, in: *IEEE Transactions on Circuits and Systems I: Regular Papers*, Volume 56, Issue 7, July 2009, pp. 1339-1348.

[12] VILLAGRASA J. P., COLOMER-FARRARONS J.,. MIRIBEL P. Ll, *Chapter 10: Bioelectronics for Amperometric Biosensors*, pp. 241-271, in: *State of the Art in Biosensors General Aspects*, InTech, 2013.

[13] *Datasheet of LTC1062*, accessed at http://cds.linear.com/docs/en/datasheet/1062fd.pdf.

[14] GRAY P. R., HURST P. J., LEWIS S. H., MEYER R. G., *Analysis and Design of Analog Integrated Circuits*, John Wiley & Sons, Inc., 2001.

[15] ENACHE A., *Circuit de prelucrare i msurare a semnalului unei celule electrochimice*, Bachelor Thesis, University Politehnica of Bucharest, 2016.

[16] *Scientific and Technical Research Report for PNCDI II 146/2014 Research Project*, First Phase, 2014.